



Leaf wax stable isotopes from Northern Tibetan Plateau: Implications for uplift and climate since 15 Ma



Guangsheng Zhuang*, Mark T. Brandon, Mark Pagani, Srinath Krishnan

Department of Geology and Geophysics, Yale University, P.O. Box 208109, 210 Whitney Avenue, New Haven, CT 06520, USA

ARTICLE INFO

Article history:

Received 8 October 2013

Received in revised form 1 January 2014

Accepted 4 January 2014

Available online xxxx

Editor: T.M. Harrison

Keywords:

n-alkane
hydrogen isotope
Qaidam
paleoaltimetry
paleoclimate

ABSTRACT

The growth of Tibetan Plateau is considered to have played a key role during the evolution of Asian climate. Our understanding of the relationship between the plateau growth and Asian climate changes is limited, however, due to the scarcity of well-dated sedimentary sequences that could provide parallel information of the evolution of elevation and climate. Here, we report a high-resolution time series record of the stable hydrogen isotopic composition of leaf-wax *n*-alkanes (δD_{n-alk}) from a continuous Neogene stratigraphic sequence (15–1.8 Ma) from the Qaidam basin on the northern Tibetan Plateau. These data are used to reconstruct the isotopic composition of meteoric waters (δD_m) and subsequently applied to interpret the history of paleotopography and climate in Qaidam.

Our results indicate four stages in the evolution of hydrology in the Qaidam basin. In Stage I (15 Ma to 10.4 Ma), δD_m gradually decreases from -24.9‰ to -75.5‰ , synchronous with a period of active tectonism. The estimated topographic growth of 2.1 ± 0.3 km is comparable to the height of Qaidam basin relative to the foreland Hexi Corridor. We note that C_3 plants were dominant in this region since the Miocene; we take this as independent evidence that this area was mountainous before the C_4 expansion in late Miocene and Pliocene. δD_m variability in subsequent stages appears to be related to shifts in dry and moist conditions and independent of topographical changes – a conclusion supported by other independent climatic records on the Tibetan Plateau. High δD_m values in Stage II (10.4 Ma to 6.9 Ma) are related to severe aridity, and Stage III (6.9 Ma to 4.1 Ma) is marked by low δD_m values, suggestive of moist conditions related to the strengthening East Asia Summer Monsoon. High δD_m values in Stage IV (4.1 Ma to 1.8 Ma) reflect a climate, drier than the present.

© 2014 Elsevier B.V. All rights reserved.

1. Introduction

The Tibetan Plateau (Fig. 1) has long served as a natural laboratory for the study of extreme topography (An et al., 2001; Currie et al., 2005; DeCelles et al., 2002, 2007; Garzione et al., 2000a; Molnar and England, 1990; Molnar et al., 1993; Murphy et al., 1997; Polissar et al., 2009; Rowley and Currie, 2006; Royden et al., 2008; Tapponnier et al., 2001). However, our understanding of the plateau still remains elusive because of the scarcity of well-dated sedimentary archives, which provides information about its paleoelevation history. Quantitative constraints on topographic development could serve as the direct means of testing tectonic models for Tibetan Plateau. For example, the Tibetan Plateau is inferred to have grown since the Late Miocene as a result of isostatic rebound in corresponding to the convective removal of over-thickened mantle lithosphere (Molnar et al., 1993), whereas a regional crustal shortening study suggests that high topography might have been

built prior to the collision (Murphy et al., 1997). Other models call for stepwise uplift, a process which would require a northward younging of high topography (Rowley and Currie, 2006; Tapponnier et al., 2001). In addition, the Tibetan Plateau is considered to have played a key role during the evolution of Asian climate (An et al., 2001; Kutzbach et al., 1989, 1993; Raymo and Ruddiman, 1992; Ruddiman and Kutzbach, 1989). Hence, the pursuit of paleoaltimetry data is also motivated by the need to better understand the interactions between tectonics and climate.

Stable oxygen isotope ($\delta^{18}\text{O}$)-based paleoaltimetry, which applies the dependence of precipitation $\delta^{18}\text{O}$ values on elevation (Clark and Fritz, 1997; Garzione et al., 2000b; Gonfiantini et al., 2001; Poage and Chamberlain, 2001), has been applied to the Himalayas and southern Tibetan Plateau (Fig. 1, Currie et al., 2005; DeCelles et al., 2007; Garzione et al., 2000a; Rowley and Currie, 2006; Saylor et al., 2009; Xu et al., 2013). These studies used carbonate minerals (i.e., pedogenic and lacustrine carbonates, aragonite shell) for reconstructing paleometeoric water $\delta^{18}\text{O}$. However, evaporative ^{18}O - and D -enrichments of soil and lake waters are substantial across the plateau (Bershaw et al., 2012; Hren et al., 2009; Quade et al., 2007, 2011; Tian et al., 2001) as indicated by

* Corresponding author. Present address: Lancaster Environment Centre, Lancaster University, Lancaster, LA1 4YQ, UK.

E-mail address: zhuangshg@gmail.com (G. Zhuang).

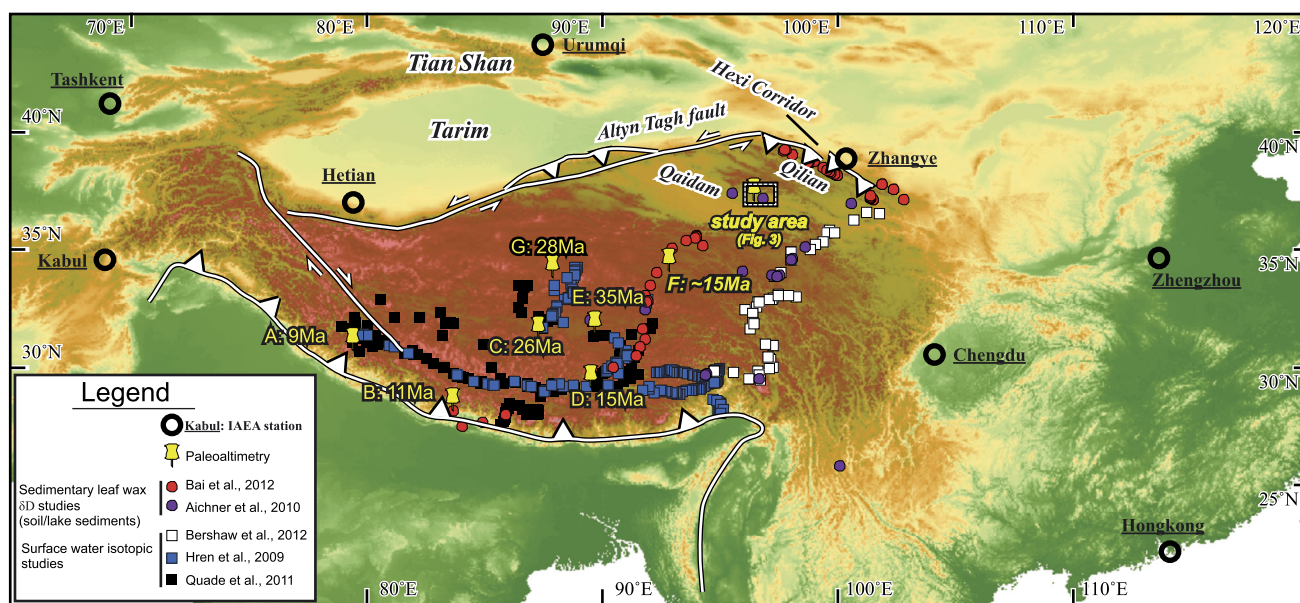


Fig. 1. Topography and principal active faults of Himalayan–Tibetan orogeny, showing locations of paleoelevation studies, isotopic studies on surface waters and sedimentary lipids, and International Atomic Energy Agency (IAEA/WMO, 2006) stations in arid central Asia and monsoon area. Paleoelevation studies with minimum timing constraints on high elevations are compiled from A: Saylor et al. (2009); B: Garzione et al. (2000a); C: DeCelles et al. (2007); D: Currie et al. (2005); E: Rowley and Currie (2006); F: Polissar et al. (2009); and G: Xu et al. (2013).

the available data (Fig. 2a, b), which leads to underestimate of paleoelevation when isotopic lapse rates are applied – $-2.8\text{‰}/\text{km}$ for $\delta^{18}\text{O}$ (Poage and Chamberlain, 2001) and $-22.4\text{‰}/\text{km}$ for δD assuming the relationship between local meteoric water $\delta^{18}\text{O}$ and δD values follow Global Meteoric Water Line (Clark and Fritz, 1997; Dansgaard, 1964; Poage and Chamberlain, 2001; Rozanski et al., 1993). A common solution to evaporative enrichment is to assume the lowest $\delta^{18}\text{O}$ values represent the least evaporated meteoric water $\delta^{18}\text{O}$ values. Paleoelevation is then estimated through comparison with either a synchronous, near sea-level reference value in an up-wind direction or the modern value at the sampling location. The wide application in Himalayas and southern Tibetan Plateau (Fig. 1, Currie et al., 2005; DeCelles et al., 2007; Garzione et al., 2000a; Rowley and Currie, 2006; Saylor et al., 2009; Xu et al., 2013) reflects that the $\delta^{18}\text{O}$ -based paleoelevation is 'a significant advance over the previous state in which there were virtually no techniques to test hypotheses regarding elevation histories of regions' (Rowley et al., 2003). However, unpredictable extent of enrichment of ^{18}O and D isotopes in surface waters and corresponding carbonates, as suggestive by deviation of surface water data points from the base line of the least evaporated meteoric waters (Fig. 2), limits the use of carbonates in reconstructing a reliable and continuous record and hence a new archive of paleometeoric waters is needed for providing higher temporal resolution for better understanding the relationship between elevation history and climate changes.

Recently, a new methodology that applies hydrogen isotope compositions of higher-plant n -alkanes ($\delta\text{D}_{n\text{-alk}}$) has attained wide application in reconstructing paleometeoric water compositions (see Sachse et al., 2012 for a summary). Studies on terrestrial plants, soil and lake sediments collected across large gradients in meteoric isotopic composition and relative humidity demonstrate that leaf-wax δD values can be used to accurately predict meteoric-water D/H compositions (Aichner et al., 2010; Bai et al., 2012; Hou et al., 2008; Sachse et al., 2004; Sauer et al., 2001; Smith and Freeman, 2006). Leaf waxes are refractory compounds ubiquitously distributed in sediments and sedimentary rocks (Pagani et al., 2000; Schimmelmann et al., 2006); their strong, covalent carbon–hydrogen bonds greatly reduce the risk

of hydrogen isotope exchange in thermally immature sediments (McInerney et al., 2011; Polissar et al., 2009; Schimmelmann et al., 2006), making them an ideal archive for studying meteoric isotopic compositions. An additional advantage of compound-specific isotope analysis is that there are useful diagnostic tests to determine if leaf waxes experienced thermal alteration. The viability of compound-specific isotope analysis in paleotopography and paleoclimate is confirmed by studies on lacustrine and fluvial sediments in South-Central Tibetan Plateau and Sierra Nevada, which give estimates consistent with other paleoelevation results (Hren et al., 2010; Polissar et al., 2009).

Leaf wax hydrogen isotope values from modern soils and lake surface sediments from the Tibetan Plateau (Aichner et al., 2010; Bai et al., 2012) track the lowest values of surface water δD_m , i.e. the least evaporated meteoric waters (Fig. 2). The measure of the difference between meteoric water and leaf wax hydrogen isotope values, expressed as the apparent fractionation factor ($\varepsilon_{n\text{-alk}/\text{m}}$) that, according to the conceptual model, incorporates influences of soil evaporation, plant transpiration, and biosynthesis processes (Polissar et al., 2009; Sachse et al., 2004, 2012; Smith and Freeman, 2006) shows no systematic trend across the plateau (Fig. 2) despite changes in precipitation amount, relative humidity, and vegetation type (Araguás-Araguás et al., 1998; Bershaw et al., 2012; Chang, 1981). This finding suggests that $\varepsilon_{n\text{-alk}/\text{m}}$ can be applied robustly to geological past regardless of changes in climate and vegetation.

The tectonic history of northern Tibetan Plateau is relatively well constrained by geological studies on syn-orogenic sediments and basement rocks (Bovet et al., 2009; Clark et al., 2010; George et al., 2001; Sun et al., 2005; Yin et al., 2002; Zheng et al., 2010; Zhuang et al., 2011a, 2011b), and isotope studies have been conducted for regional climatic reconstructions (Dettman et al., 2003; Fan et al., 2007; Graham et al., 2005; Hough et al., 2011; Kent-Corson et al., 2009; Zhuang et al., 2011a). Here, we present lipid wax $\delta\text{D}_{n\text{-alk}}$ measurements from a densely sampled late Cenozoic stratigraphic sequence in the Qaidam basin on the northern Tibetan Plateau (Figs. 1, 3, and 4). We then convert $\delta\text{D}_{n\text{-alk}}$ values to δD_m by applying the modern apparent fractionation factor established between meteoric waters and sedimentary lipids

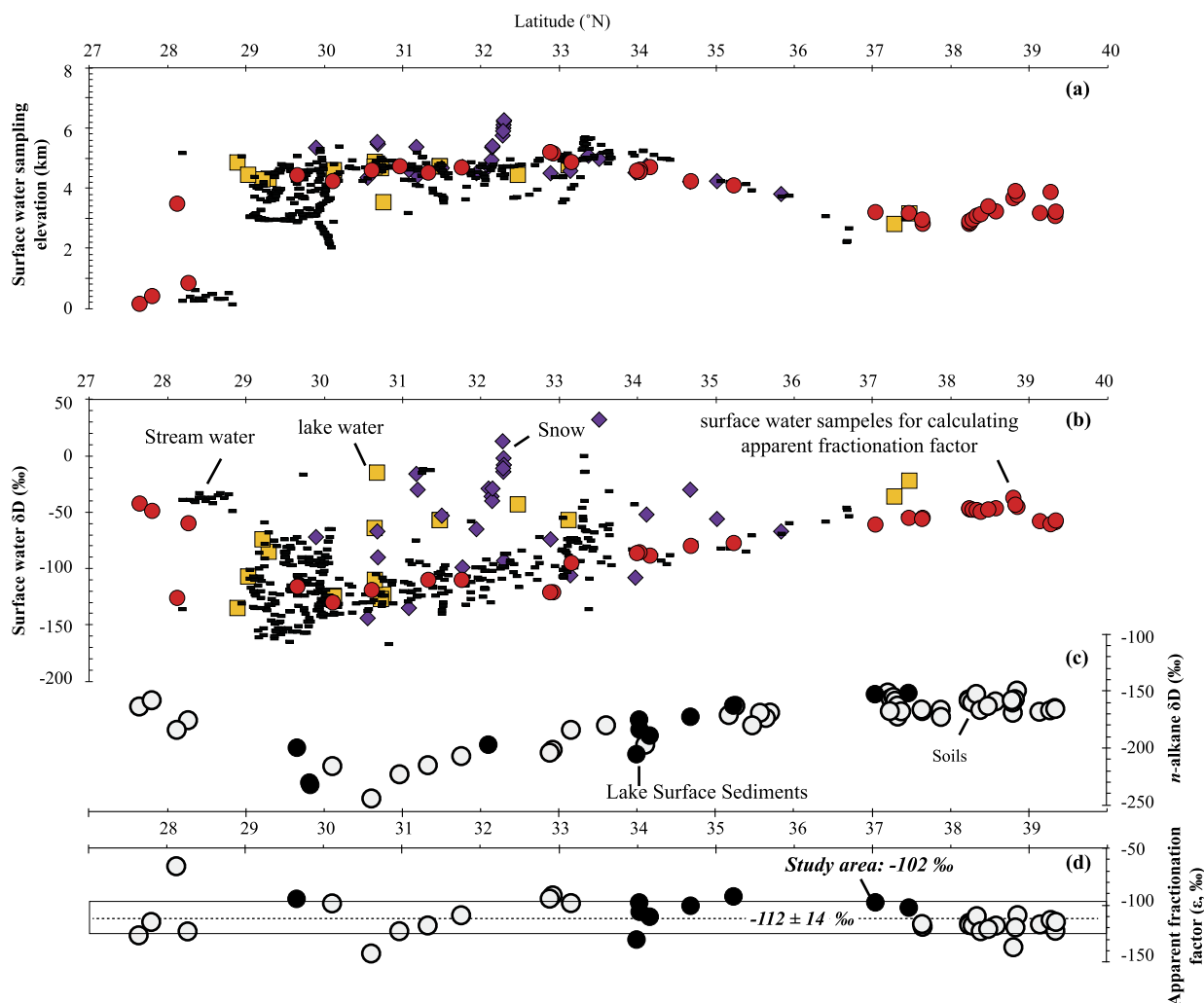


Fig. 2. Isotope data on surface waters (δD_m) and lipid waxes (δD_{n-alk}), compiled from Aichner et al. (2010), Bai et al. (2012), Bershaw et al. (2012), Hren et al. (2009), and Quade et al. (2011). (a) and (b) are plots of sampling elevation and surface water δD_m values against latitude. Black rectangles, brown squares, purple diamonds, and red circles denote small streams, lake waters, snows, and streams which are chosen to calculate the apparent fractionation factor. (c) and (d) show n -alkane hydrogen isotope values (δD_{n-alk}) and apparent fractionation factors ($\epsilon_{n-alk/m}$) for soils (gray circle) and lake sediments (black circle) against latitude. The apparent fractionation factors are compiled from reported values that have paired stream water samples (Bai et al., 2012) and our calculations based on the data of n -alkane hydrogen isotope values reported in Aichner et al. (2010). (For interpretation of the references to color in this figure legend, the reader is referred to the web version of this article.)

(Fig. 2d). Within reconstructed tectonic-climatic context, we examine and test for signals related to the uplift and climate.

2. Geology, stratigraphy, and climate

The Cenozoic Qaidam basin is a non-marine, intermontane basin on the northern Tibetan Plateau which is bound by the sinistral strike-slip Altyn Tagh fault (ATF) to the northwest, the Qilian Shan fold-thrust belt to the northeast (Fig. 1). The Qaidam basin is located at 2800–3500 m above sea level, in contrast to 1000–1500 m for the Hexi Corridor in the north. The Qaidam basin contains thick successions of Eocene–Quaternary deposits that document two phases of tectonic events (Yin et al., 2002; Zhuang et al., 2011b). Eocene-age coarse clastic deposits along the northern Qaidam basin (Yin et al., 2002; Zhuang et al., 2011b), together with fast erosion on basement rocks (Clark et al., 2010), were used as evidence supporting the early Cenozoic faulting related to the far-field response of Indo-Asia collision. In the Middle to Late Miocene, the deformation was reactivated on old structures and propagated towards the north and northeast (Bovet et al., 2009; Clark et al., 2010; Lease et al., 2011; Zheng et al., 2010; Zhuang et al., 2011b). This phase of active tectonism

is well documented by post-Middle Miocene coarse clastic sequences in the Qaidam basin, Hexi Corridor, and intermontane basins within the Qilian Shan (Bovet et al., 2009; Sun et al., 2005; Zhuang et al., 2011b), accelerated crustal shortening (Zhou et al., 2006), and rapid erosion on basement rocks (George et al., 2001; Jolivet et al., 2001; Zheng et al., 2010).

We collected samples from the Miocene–Quaternary strata (Figs. 3 and 4) that are well exposed in the Huaitoutala (HT) section in the northeastern Qaidam basin (Fig. 3). The HT section with a thickness of ca. 5300 meter, crops out in the north limb of an anticline and was studied in detail for basin analysis (Zhuang et al., 2011b). Based on sedimentary environment and facies analysis, the HT section can be divided into six units (Fig. 4). Unit 1 starts with a coarsening-upward sequence ranging from a reddish paleosol, through fine- to coarse-grained sandstone, to 80-meter-thick pebble–cobble conglomerate and is dominated by conglomerates and coarse sandstone upsection. The sedimentary and stratigraphic characteristics support that this unit was mainly formed in alluvial fan environment. Unit 2 is dominated by meandering river systems that are characterized by lenticular channel deposits and thick packages of overbank mudstone and siltstone. Unit 3 is characterized by multiple-channel deposits with medium- to coarse-

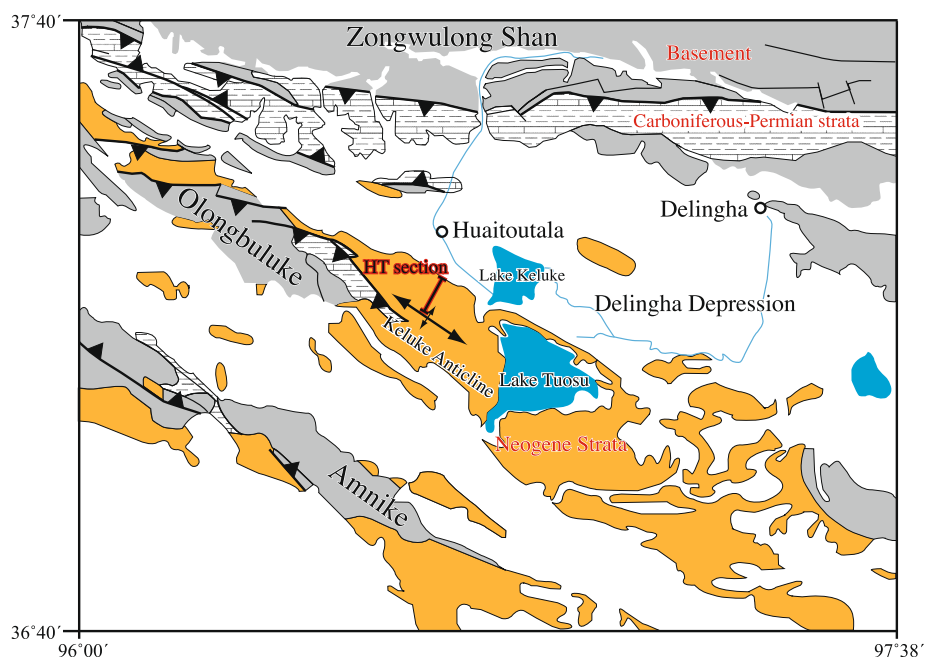


Fig. 3. Geologic map of the northeastern Qaidam basin (modified from Zhuang et al., 2011a). Samples were taken from the Neogene strata at the Huaitoutala (HT) section on the north limb of the Keluke anticline.

grained sandstone and minor overbank siltstone and mudstone which are interpreted as braided river systems. Unit 4 is an open lacustrine facies and dominated by massive to laminated mudstone with minor tabular fine-grained sandstone. Units 5 and 6 are braided river systems and Unit 6 has pebble–cobble conglomerates (Fig. 4). The chronology for the HT section was established by magnetostratigraphic and paleontology studies (Fang et al., 2007; Wang et al., 2007); the HT section was measured along the very canyon of the magnetostratigraphic study and age assignments for samples were refined by lithological correlation between the HT section and the magnetostratigraphic column with help of fossil assemblages (Fang et al., 2007; Wang et al., 2007; Zhuang et al., 2011a, 2011b).

The modern climate in central Asia, including the Qaidam, is dominated by dry air masses characterized by ^{18}O - and D -enriched summer precipitation (Fig. S1; Araguás-Araguás et al., 1998; Rozanski et al., 1993; Tian et al., 2001, 2003). High $\delta^{18}\text{O}$ and δD values for precipitation are considered to be related to arid conditions and increasing contributions of recycling continental air masses (Araguás-Araguás et al., 1998). The region to the southeast is under the control of monsoon systems (Figs. 1 and S1), which is characterized by isotopically depleted summer precipitation (Araguás-Araguás et al., 1998; Tian et al., 2001) associated with high precipitation amount – the so-called “Amount Effect” (Dansgaard, 1964; Rozanski et al., 1993). Isotopic data from meteorological stations of International Atomic Energy Agency (IAEA) in this region support a linear relationship between δD and precipitation with a slope of $-0.215\text{‰}/\text{mm}$, ranging from -0.101 to $-0.334\text{‰}/\text{mm}$ (IAEA/WMO, 2006). The northeastern Qaidam basin lies on the boundary separating the humid monsoonal area to the southeast and dry central Asia to the northwest. And it has a relative humidity between 40% and 60% and receives more than 91% of rainfall in May to September (Tian et al., 2001).

3. Analytical method

We collected forty-two paleosol, lacustrine, and fluvial mudstone samples (Fig. 4). Fresh rock samples were collected after removing the surface layers to avoid any possible contamination

from recent organic material. In the laboratory, the outer 0.5–1 cm of each sample was removed with a Dremel® high-speed tungsten carbide bit and leached with dichloromethane (DCM). Samples were broken into small fragments and surfaces with any chemical alteration were abraded with the Dremel tool. Samples were powdered and freeze dried for over 48 hours.

3.1. Organic matter extraction

Total lipids were extracted using Soxhlet extractors with a solvent mixture of dichloromethane (DCM)/methanol 2:1 (v/v) for 48 hours. Total lipid extracts (TLE) were evaporated using a Zymark Turbovap II solvent evaporator under a stream of purified nitrogen until dry. Total lipid extracts were separated into compound classes using ~ 4.0 g of pre-extracted, activated ($@200^\circ\text{C}$ for 2 hours) silica gel. Organic compounds in TLE were separated into apolar, intermediate, and polar fractions by using 4 mls hexane, 4 mls DCM, and 4 mls methanol, respectively. N-alkanes are contained in the apolar portion.

3.2. Compound characterization

N-alkane abundances were determined using a Thermo Trace 2000 gas chromatography-flame ionization detector (GC-FID) fitted with a programmable-temperature vaporization (PTV) injector and a fused silica, DB-1 stage column (60 m long, 0.25 mm i.d., 0.25 μm film thickness). Samples were carried by helium at a flow of 2 ml/min. GC oven temperature was ramped from 60°C (holding for 1 min) to 320°C at $15^\circ\text{C}/\text{min}$ and hold at 320°C for 20 min. N-alkanes were identified through comparison of elution times with laboratory standard mixture of $n\text{C}_{20}$, $n\text{C}_{25}$, $n\text{C}_{28}$, and $n\text{C}_{30}$.

Individual n -alkane peak areas were calculated using Xcalber software. The carbon preference index (CPI) values were determined using the following equation:

$$\text{CPI} = \frac{1}{2} \frac{\sum A(23-33)\text{odd} + \sum A(25-35)\text{odd}}{\sum A(24-34)\text{even}} \quad (1)$$

where A in above equation corresponds to the area of the individual n -alkane peak from the chromatograph trace.

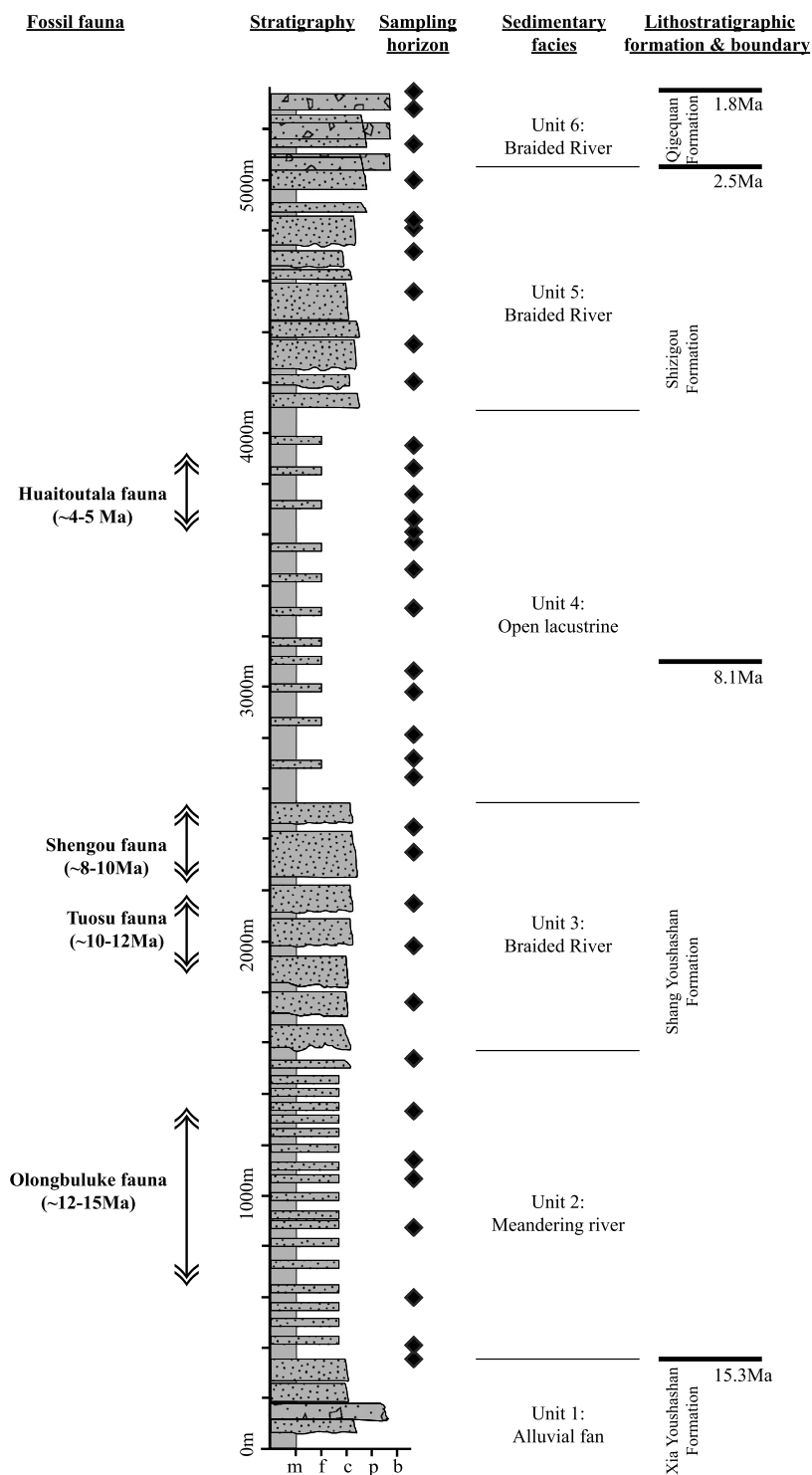


Fig. 4. The stratigraphic column of HT section with interpretation of sedimentary environments for major units. Also shown are the sampling horizons and fossil fauna (Wang et al., 2007). Absolute age constraints (15.3 Ma, 8.1 Ma, and 2.5 Ma) for lithostratigraphic boundaries between Xia Youshashan, Shang Youshashan, Shizigou, and Qigequan formations are interpreted from Fang et al. (2007).

3.3. Hydrogen isotope analysis

Measurements of compound-specific hydrogen isotope values were performed using a Thermo Trace 2000 GC coupled to a Finnigan MAT 253 isotope ratio mass spectrometer (IRMS) interfaced with a Finnigan GC-C combustion III interface. The GC column and carrier flow conditions were identical to above. Compounds were separated on the GC with a temperature program from 90 °C (held for 2 min) to 170 °C at 14 °C/min, to 300 °C at 3 °C/min, and then

to 325 °C at 14 °C/min with an isothermal holding of 10 min. The H_3^+ factor (Sessions et al., 2001) was measured daily prior to δD analysis, with a mean value of 16.0 ± 0.3 (1σ) for the measurement periods. The drift of the instrument was routinely monitored and individual n -alkane isotope ratios were corrected to n -alkane reference materials (Mix A3, A. Schimmelmann, Indiana University Bloomington). Most samples were analyzed in duplicate with average analytical precision of 2.4 to 2.6‰ for δD (Table 1). Isotopic

Table 1 δD values of *n*-alkanes and estimated paleometeoritic waters.

Sample	Age (Ma) ^a	$\delta D_{n\text{-alk}}$ (‰)								δD_m^b (‰)	CPI ^c
		<i>n</i> C ₂₇	Error (1 σ)	<i>n</i> C ₂₉	Error (1 σ)	<i>n</i> C ₃₁	Error (1 σ)	<i>n</i> C ₃₃	Error (1 σ)	Weighted-mean	
07HTB045	15.00	−115.3	6.7	−118.2	0.4	−126.6	0.7	−123.7	1.7	−124.6	11.0
07HT009	14.88	−140.3	5.3	−134.2	6.2	−137.6	2.0	−123.0	3.7	−135.3	8.4
07HT056	14.48	−153.9	1.3	−144.5	0.4	−141.6	1.8	−123.2	1.1	−142.0	10.3
07HT082	13.88	−147.2	0.6	−143.8	0.2	−148.6	0.3	−132.4	0.1	−145.2	7.0
07HT113	13.47	−156.6	1.1	−151.5	0.5	−156.3	1.2	−152.7	0.2	−154.3	6.6
07HT122	13.31	−160.5	3.9	−154.8	2.7	−154.9	0.8	−143.6	1.2	−154.2	6.4
07HT142	12.89	−134.1	5.9	−135.4	4.1	−137.0	2.2	−127.5	4.1	−135.3	7.1
07HT159	12.44	−103.6	n/a	−125.3	n/a	−139.8	n/a	−120.8	n/a	−130.5	6.6
07HT169	11.96	−158.3	2.7	−154.8	0.6	−152.8	0.6	−145.2	0.2	−153.4	8.7
07HT187	11.48	−158.0	0.7	−162.8	0.8	−162.1	2.4	−157.9	0.6	−160.2	5.8
07HT204	11.12	−157.8	2.5	−158.5	2.6	−158.6	0.5	−146.0	3.2	−156.7	6.8
07HT216	10.69	−174.1	0.4	−173.9	0.7	−171.3	0.7	−157.7	1.8	−170.1	16.6
07HT223	10.39	−181.6	1.4	−173.0	1.4	−164.7	1.3	−156.2	2.6	−169.1	7.8
07HT233	9.71	−160.5	0.7	−148.2	1.7	−139.8	1.0	n/a	n/a	−147.4	5.3
07HT244	9.45	−143.7	0.2	−143.6	0.2	−142.4	0.0	−126.5	1.1	−140.3	8.5
07HT255	9.12	−117.3	0.5	−117.6	0.5	−116.2	0.6	−116.4	0.0	−116.9	7.9
07HT282	8.53	−115.9	2.6	−116.2	2.6	n/a	n/a	−123.0	1.5	−118.1	10.6
07HT292	8.24	−151.2	n/a	−136.6	n/a	−138.2	2.8	−124.2	n/a	−137.4	16.7
07HT328	7.38	−125.5	n/a	−116.9	4.9	−113.6	7.7	−105.9	n/a	−114.4	35.7
07HT355	6.85	−129.7	n/a	−128.7	n/a	−126.1	n/a	−120.0	n/a	−125.7	6.6
07HT373	6.47	−212.9	7.0	−216.2	7.8	−190.8	7.7	−184.3	7.2	−208.5	2.5
07HT379	6.33	−165.6	0.9	−173.6	0.3	−164.4	1.5	n/a	n/a	−168.0	3.8
07HT388	6.16	−155.5	0.3	−155.9	0.1	−191.9	6.2	−140.6	9.9	−168.0	4.6
07HT402	5.82	−136.5	3.3	−136.3	0.9	n/a	n/a	n/a	n/a	−136.4	9.3
07HT420	5.45	−138.6	n/a	−143.1	6.2	−144.1	5.7	−129.6	4.3	−142.7	21.0
07HT432	5.14	−173.8	0.2	−170.2	1.0	−167.1	0.7	−156.2	1.0	−167.2	7.1
07HT469	4.46	−168.8	n/a	−165.4	n/a	−165.6	n/a	−165.6	n/a	−166.0	4.2
07HT483	4.14	−185.5	3.4	−172.2	4.9	−149.4	5.0	−134.6	6.8	−170.8	4.8
07HT501	3.68	−145.5	3.6	−135.8	2.4	−148.5	2.4	−157.4	2.0	−145.1	15.3
07HTA005	3.33	−150.6	2.1	−149.9	2.3	−143.4	3.4	−144.8	0.2	−146.4	8.9
07HTA015	3.12	−139.8	0.1	−132.7	2.7	n/a	n/a	n/a	n/a	−134.7	9.5
07HTA018	3.08	−158.0	3.0	−152.0	2.5	−142.2	0.7	−138.2	2.4	−150.4	2.5
07HTA022	2.71	−124.2	1.4	−130.0	2.3	−132.7	n/a	−134.8	n/a	−130.3	7.9
07HTA037	2.37	−162.5	0.3	−154.5	0.5	n/a	n/a	−144.8	1.3	−154.4	8.6
07HTA050	1.99	−131.2	17.2	−134.6	11.3	−144.0	9.0	−132.9	4.2	−137.8	8.5
07HTA057	1.80	−144.7	0.1	−147.5	1.3	−153.3	1.8	−148.9	1.6	−150.5	15.3
Average	–	–	2.6	–	2.4	–	2.5	–	2.5	–	9.3

n/a: No replicate analysis and hence no reports for mean and standard error.

^a Assignment of absolute ages is based on the magnetostratigraphic study (Fang et al., 2007) and fossil fauna (Wang et al., 2007).^b Paleometeoritic water δD_m values were calculated by applying the locally established apparent fractionation factor ($\epsilon_{n\text{-alk}/m} = -102\text{‰}$).^c Carbon preference index (CPI) is calculated by using Eq. (1).

compositions were determined by using this equation:

$$\delta D = \left(\frac{R_{\text{sample}}}{R_{\text{standard}}} - 1 \right) \quad (2)$$

where *R* stands for the D/H ratio of samples and standards. δD values are reported relative to Vienna Standard Mean Ocean Water (VSMOW) and expressed in per mil (‰).

4. Results

N-alkanes display prominent odd-over-even feature with *n*C₂₇, *n*C₂₉, *n*C₃₁, and *n*C₃₃ representing the most abundant compounds, indicative of terrestrial higher plant input (Eglinton and Hamilton, 1967; Tipple and Pagani, 2007). CPI values, ranging from 2.5 to 35.7 (Table 1), suggest minimal thermal alteration (Cooper and Bray, 1963; Marzi et al., 1993; Tissot and Welte, 1978), implying that our samples had not gone through post-depositional thermal degradation. About 200 detrital apatite grains from 8 samples throughout the HT section were analyzed for (U–Th)/He study (Zhuang et al., 2009; unpublished data). Even the bottom sample with a depositional age of ca. 15.3 Ma was not fully reset, as there are lots of grains that have He ages ranging between 100 and 250 Ma. Hence, our detrital apatite (U–Th)/He thermochronology data do not support thermally re-setting (Zhuang et al., 2009), and indicate that maximum burial temperatures was less than ~70 °C (Reiners and Brandon, 2006).

4.1. Isotopic results

Thirty-six samples have high molecular concentrations to obtain measurable stable hydrogen isotope values of *n*-alkanes. We report stable hydrogen isotope values for *n*C₂₇, *n*C₂₉, *n*C₃₁, and *n*C₃₃ (Table 1; Fig. 5). The four compounds show similar isotopic trends throughout this time series (Fig. 5). δD values range from −103.6‰ to −216.2‰ (Table 1). We assessed our results with a local regression method that uses weighted linear least squares and a 2nd degree polynomial kernel (Loader, 1999) with a span specified at 10% of the total number of data points during the smoothing (Fig. 5). Weighted mean values based on δD of these four *n*-alkanes were calculated using the equation:

$$\Delta D_{n\text{-alk}} = \frac{\sum A_i * \delta D_i}{\sum (A_i)} \quad (3)$$

where *A* in above equations corresponds to the area of the individual *n*-alkane peak from the chromatograph trace with *i* (= 27–33) indicating carbon atoms.

The resulting isotopic record can be divided into four temporal stages (Fig. 6). For Stage I (15–10.4 Ma), the weighted mean $\delta D_{n\text{-alk}}$ values display gradual decrease from −124.6‰ to −170.1‰. Stage II (10.4–6.9 Ma), within the lacustrine facies (Figs. 4 and 6), is separated by an abrupt increase from Stage I and has high $\delta D_{n\text{-alk}}$ values, varying between −147.4‰ to −114.4‰. Samples in Stage III (6.9–4.1 Ma) were collected from

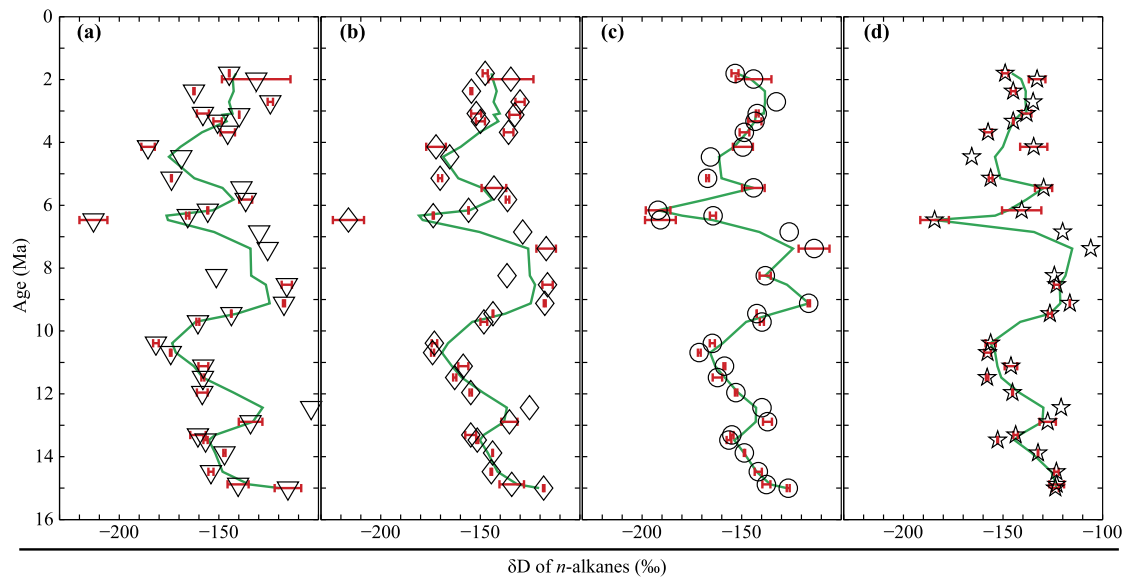


Fig. 5. Stable hydrogen isotope values (δD) for n -alkanes nC_{27} (a), nC_{29} (b), nC_{31} (c), and nC_{33} (d). Red bars indicate one standard error. Temporal trends (green lines) in δD_{n-alk} are assessed by a local regression method that uses weighted linear least squares and 2nd polynomial kernel (Loader, 1999) with a span of 10%. δD values for nC_{27} , nC_{29} , nC_{31} , and nC_{33} show high co-variation throughout the whole time series. The data points that do not have error bars are samples having one analysis due to low n -alkane concentrations. (For interpretation of the references to color in this figure legend, the reader is referred to the web version of this article.)

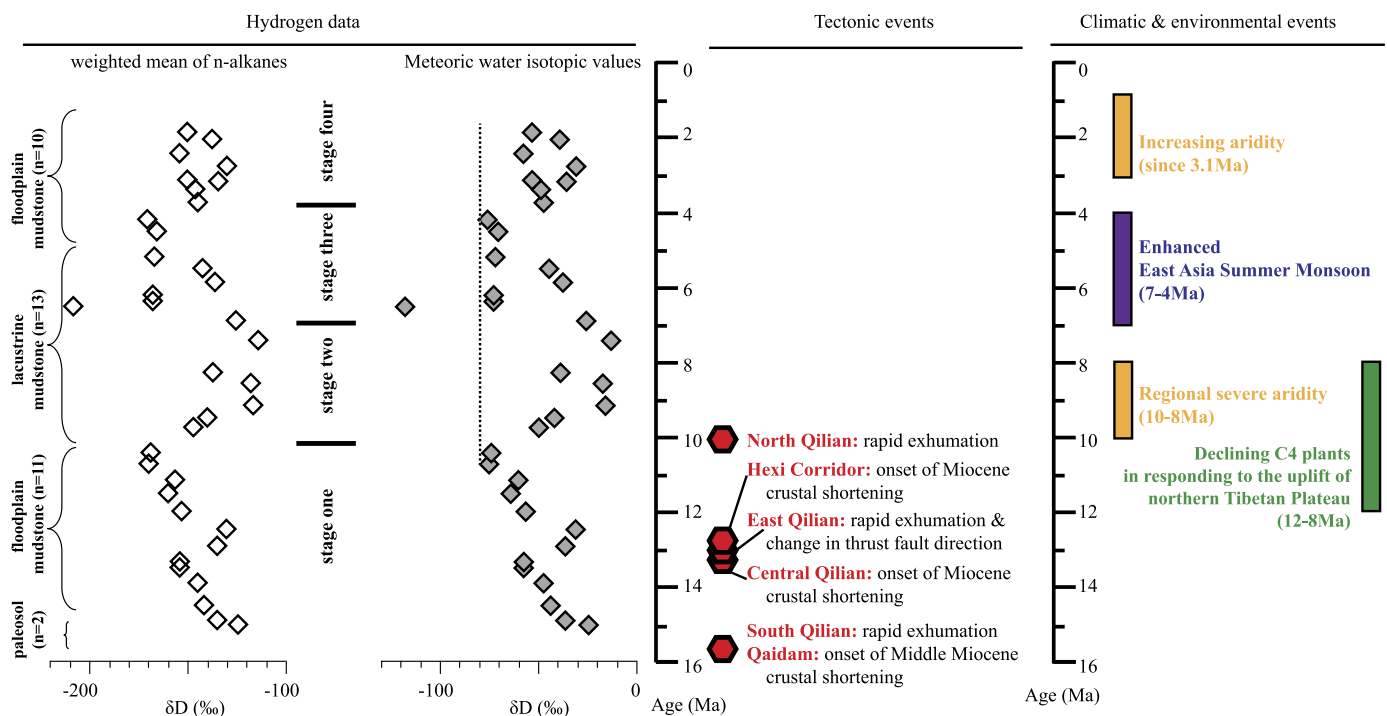


Fig. 6. Weighted mean of n -alkane δD_{n-alk} and reconstructed meteoric water δD_m with summaries on tectonic, climatic, and environmental events. Note changes in sedimentary facies are not coeval with changes in δD_m . Please refer to the text for more detailed discussions. The dotted line in meteoric water isotopic values serves as a baseline for comparing δD_m in Stages II through IV to those prior to 10.4 Ma. Studies which support the Middle–Late Miocene active tectonism are compiled from Bovet et al. (2009) for Hexi Corridor, George et al. (2001) and Zheng et al. (2010) for North Qilian, Lease et al. (2007, 2011) for East Qilian, Sun et al. (2005) for central Qilian, and Zhuang et al. (2011b) for South Qilian and Qaidam. Isotopic studies supporting periods of strengthened aridity at 10–8 Ma and since 3.1 Ma are summarized from Dettman et al. (2003), Hough et al. (2011), Zhuang et al. (2011a), and Heermance et al. (2013). Studies on enhanced East Asia Summer Monsoon and declining C_4 plants are referred to Passey et al. (2009) and Jia et al. (2012), respectively.

both lacustrine and fluvial facies, and starts with a decrease in δD_{n-alk} values, ranging between -136.4‰ and -170.8‰ that are lower compared to samples prior to and after this stage. Stage IV ranges from 4.1 Ma to the end of the record (1.8 Ma) where δD_{n-alk} values become higher and vary between -134.7‰ to -150.5‰ .

4.2. Long-term hydrological evolution

We calculated the regional and local apparent fractionation factors based on data sets of δD values of modern soil and lake surface sediments and paired meteoric waters (Fig. 2). Aichner et al. (2010) reported individual n -alkane δD_{n-alk} values for a recent

lake surface sediment sample in this area with an average $\delta D_{n\text{-alk}}$ value of -152‰ . The weighted mean of meteoric water $\delta^{18}\text{O}$ in the northeastern Qaidam basin is reported to be -6.5‰ with a slope of 8.4 for the local meteoric water line (Tian et al., 2001). The local meteoric water δD_m would be ca. -55‰ ; this value is much higher than δD_m (-81‰) used by Aichner et al. (2010) which was derived from the online isotope precipitation calculator (Bowen and Revenaugh, 2003). We suggest that δD_m of -55‰ is more representative, as this value is based on yearly observations (Tian et al., 2001). With δD_m value of -55‰ , we calculate the local apparent fractionation factor between leaf wax and meteoric waters ($\varepsilon_{n\text{-alk/m}}$) to be -102‰ , using the relationship:

$$\varepsilon_{n\text{-alk/m}} = \frac{\delta D_{n\text{-alk}} + 1}{\delta D_m + 1} - 1 \quad (4)$$

where $\delta D_{n\text{-alk}}$ and δD_m are weighted-mean δD values of n -alkanes and δD values of meteoric waters (Figs. 2b and 2c). The calculated $\varepsilon_{n\text{-alk/m}}$ is consistent with a recent study on modern soils in the Qilian Shan to the north that have an average value of $-118 \pm 6\text{‰}$ ($n = 17$) (Bai et al., 2012). This value is also in the range of the mean ($-112 \pm 14\text{‰}$) of available apparent fractionation factors across the plateau (Fig. 2d).

By applying the established $\varepsilon_{n\text{-alk/m}}$ in our study area, we convert weighted mean $\delta D_{n\text{-alk}}$ values to paleometeoric water δD_m values (Fig. 6). In Stage I (15–10.4 Ma), δD_m gradually decreases from -24.9‰ to -75.5‰ by -50.6‰ . And then δD_m values become higher and range between -13.4‰ and -50.2‰ in Stage II (10.4–6.9 Ma). In Stage III (6.9–4.1 Ma), δD_m values become lower and vary between -37.9‰ and -76.3‰ . In Stage IV (4.1–1.8 Ma), δD_m values vary between -31.2‰ and -53.7‰ , higher than the present δD_m of -55‰ (Tian et al., 2001).

5. Discussion

5.1. Evaluating the reconstruction of paleometeoric water compositions

A key question in sedimentary leaf wax hydrogen isotope studies is whether the apparent fractionation factor ($\varepsilon_{n\text{-alk/m}}$) established based on modern soil/sediment and meteoric water is applicable to the geological past. This is a very common challenge facing paleoclimate studies. In this study we suggest that our calculated $\varepsilon_{n\text{-alk/m}}$ is a very robust establishment and hence can be used to convert sedimentary leaf wax $\delta D_{n\text{-alk}}$ values to paleometeoric water δD_m values due to following reasons. We observed that $\varepsilon_{n\text{-alk/m}}$ values show no systematic variation across the Tibetan Plateau (Fig. 2d) despite great changes in elevation, precipitation amount, relative humidity, and vegetation type (Bershaw et al., 2012; Chang, 1981; Tian et al., 2003). This finding is consistent with observations from a transect across the southwestern United States (Hou et al., 2008) and would suggest that combined impact of environmental factors, i.e. the soil evaporation, the plant transpiration, and biosynthesis processes, is relatively small, though each influencing factor would contribute very differently, if considered separately (Bi et al., 2005; Chikaraishi and Naraoka, 2003; Chikaraishi et al., 2004; Douglas et al., 2012; Hou et al., 2008; Liu and Yang, 2008; McInerney et al., 2011; Polissar and Freeman, 2010; Polissar et al., 2009; Sachse et al., 2012, 2004; Sauer et al., 2001; Smith and Freeman, 2006). For example, hydrogen isotope ratios in leaf waxes of grasses are insensitive to transpiration, which was confirmed by both experimental and field studies (Hou et al., 2008; McInerney et al., 2011). Whereas the soil evaporation enriches deuterium in soil water and decrease the apparent fractionation factor, especially in arid areas (Douglas et al., 2012; Hou et al., 2008; Polissar and Freeman, 2010; Smith and Freeman, 2006). Studies to date reveal differences in biosynthetic fractionation in different plant groups. Hydrogen isotopes in C_4 grasses

are ca. 15‰ higher than C_3 grasses but ca. 20‰ lower than C_3 trees if grown in same conditions (Chikaraishi and Naraoka, 2003; Chikaraishi et al., 2004; McInerney et al., 2011; Sachse et al., 2012; Smith and Freeman, 2006). We suggest that the relatively invariant fractionation factor across the Tibetan Plateau could be related to the derivation of sedimentary leaf waxes in soils or lake sediments from a broad drainage area, which smooth out differences introduced by specific taxa and soil evaporation and plant transpiration.

5.2. Establishment of high Northern Tibetan Plateau

Our 13 million year-long stable hydrogen isotopic record archives the paleohydrologic evolution of the Qaidam basin (Fig. 6). The most conspicuous feature is the gradual decrease in δD_m during Stage I. Competing factors, including changes in moisture source and/or precipitation, vegetation type, temperature variation associated with global change, and uplift-driven fractionation all could contribute to this decrease. Regarding moistures or precipitation, a decrease in hydrogen isotope value would require a change from dry to wet in climate. However, isotopic studies and pollen records in this region support a general drying which culminated between 10 and 8 Ma (Dettman et al., 2003; Fan et al., 2007; Hough et al., 2011; Kent-Corson et al., 2009; Miao et al., 2010; Zhuang et al., 2011a). In terms to vegetation type, carbon isotopic studies on fossil enamel suggest no significant change in vegetation since the Early Miocene in this region (Wang and Deng, 2005; Zhang et al., 2012), implying little or no contribution from the change in taxon-specific biosynthetic fractionation.

The decrease in hydrogen isotopes in Stage I occurred in a period of the climatic transition from the Middle Miocene Climatic Optimum to the “ice house” (Flower and Kennett, 1994; Zachos et al., 2001). Observations from IAEA/WMO stations in this region gives a coefficient for $\delta^{18}\text{O}$ -temperature ranging between $0.349\text{‰}/^\circ\text{C}$ to $0.555\text{‰}/^\circ\text{C}$ (Araguás-Araguás et al., 1998) or $2.5\text{‰}/^\circ\text{C}$ to $4.1\text{‰}/^\circ\text{C}$ for δD -temperature that is converted from the gradient of $\delta^{18}\text{O}$ -temperature by multiplying the slope of local meteoric water line (Dansgaard, 1964; Rozanski et al., 1993). These isotope-temperature gradients are slightly smaller than the global mean of $0.69\text{‰}/^\circ\text{C}$ and $5.6\text{‰}/^\circ\text{C}$ for $\delta^{18}\text{O}$ and δD , respectively (Dansgaard, 1964). The range between $2.5\text{‰}/^\circ\text{C}$ and $4.1\text{‰}/^\circ\text{C}$ for δD would suggest a minimum temperature drop of 12.3°C corresponding to the decrease of 50.6‰ in δD_m . Though it is difficult to evaluate to what extent the global cooling contributes to this temperature drop, we suggest that it was not the determinant factor. We note that the onset of this decrease (>15 Ma) was slightly earlier than the global climatic transition at ca. 14.8 Ma (Flower and Kennett, 1994; Zachos et al., 2001). And a compilation of temperature records from European continent which provides an analogue in high northern latitude area suggests that the mean annual temperature was possibly dropping no more than $3\text{--}4^\circ\text{C}$ during this period (Mosbrugger et al., 2005) and our calculation of temperature drop of 12.3°C is only a minimum. Based on discussions above, we suggest that the steady decrease in δD_m reflects a scenario of gradual deuterium-depletion in precipitation related to the topographic growth (Fig. 7) and the calculated temperature drop ($>12.3^\circ\text{C}$) was a result of uplift.

5.2.1. Middle-Late Miocene active tectonism and uplift

Major evidence supporting the Middle-Late Miocene active tectonism and surface uplift come from a variety of sedimentary, structural, and thermochronological studies in and around the northern Tibetan Plateau (Figs. 6 and 8a). Basin analysis in Qaidam reveals a basin-wide transition in facies from low- to high-gradient depositional environment around the Middle Miocene and subsequent deposition of coarse clastic sediments, which is accompa-

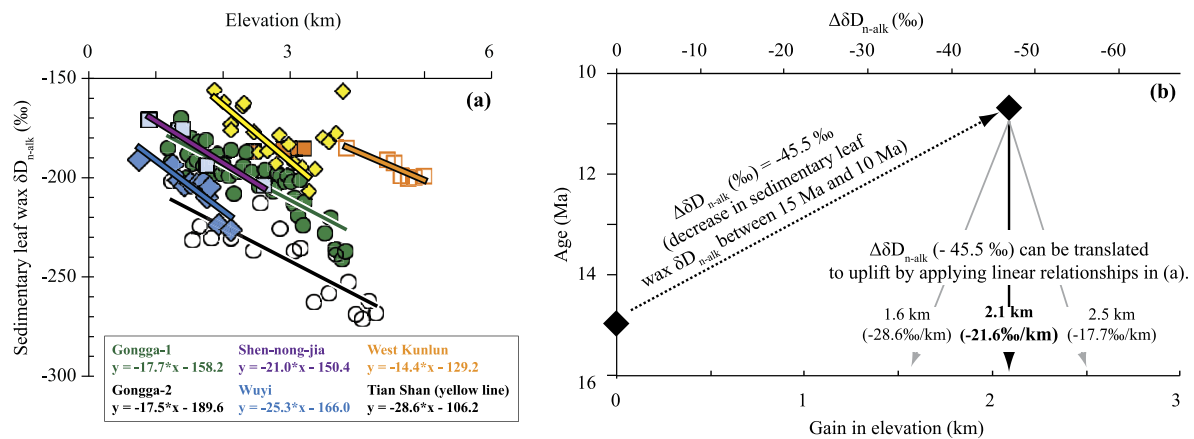


Fig. 7. Estimating surface uplift in the Qaidam basin. (a) Empirical linear relationships between sedimentary leaf wax δD_{n-alk} and elevation are compiled from Bai et al. (2011) for West Kunlun and Gongga-2, Jia et al. (2008) for Gongga-1, and Luo et al. (2011) for Tian Shan, Shen-nong-jia and Wuyi. (b) The decrease in sedimentary leaf wax δD_{n-alk} ($\Delta \delta D_{n-alk} = -45.5\text{‰}$) between 15 Ma to 10.4 Ma can be used to estimate the change in elevation by applying lapse rates summarized in (a). The gain in elevation ranges between 1.6 km and 2.5 km with a mean of 2.1 km by applying an average lapse rate of -21.6‰/km . See the text for more discussions.

nied by the expansion of faulting-induced flexural accommodation around 15 Ma in the northeastern Qaidam basin (Zhuang et al., 2011b). By using magnetostratigraphy, Sun et al. (2005) dated a sedimentary sequence of molasse deposits in the central Qilian Shan near the Altyn Tagh fault (Fig. 1), which constrained the accumulation of conglomerates between 13.7 and 9 Ma, suggesting a rapid uplift of central Qilian Shan during this time. In the north of Qilian Shan, Bovet et al. (2009) conducted a regional basin analysis in the western Hexi Corridor and identified a change in facies from low to high energy depositional environment at ca. 11 Ma, which was interpreted to support the onset of crustal shortening in the frontal North Qilian Shan prior to the Late Miocene. Findings from sedimentary records are consistent with regional thermochronological studies which reveal rapid uplift of western and central segments of north frontal Qilian Shan at 20–10 and 10 Ma, respectively (Fig. 8a; George et al., 2001; Johnstone et al., 2009; Zheng et al., 2010). Thermochronological studies from the Jishi Shan and Laji Shan to the southeast of Qilian Shan and isotopic studies in intermontane basins reveal a change in fault orientation and topographic growth by 13 Ma (Fig. 8a; Hough et al., 2011; Lease et al., 2011; Lease et al., 2007). The activation of Qilian Shan fold-thrust belt was synchronous with the transition in kinematics of the Altyn Tagh fault from dominant extrusion to distributed crustal shortening in the Middle Miocene (Yue et al., 2003, 2004), consistent with a regional structural study that reveals intense crustal shortening since the Miocene (Zhou et al., 2006).

5.2.2. High topography-related transition in paleoecology and paleoenvironment

Surface uplift in the Middle-Late Miocene is supported by paleoecology and paleoenvironment studies. Jia et al. (2012) presented isotopic evidence supporting a decline in C_4 plants that are favored under warm conditions at low elevations from $>18\%$ prior to 12–8 Ma to 10% afterwards (Fig. 6). The decline in C_4 plants was attributed to the regional temperature drop related to the topographic growth. Regional temperature drop is consistent with the Middle to Late Miocene pollen record that shows decreasing thermophilic taxa, accompanied by increasing xerophytic taxa since 14 Ma (Miao et al., 2010). Our inference of temperature drop is in line with these studies. Moreover, the inference of the decline in C_4 plants from molecular carbon isotopic study (Jia et al., 2008) is also consistent with carbon isotope studies on fossil tooth enamel and paleosol carbonates which reveal dominant C_3 plants in the northern Tibetan Plateau since the early Miocene (Wang and Deng, 2005; Zhang et al., 2012). This is in strikingly contrast with

carbon isotopic evidence supporting the C_4 expansion on the adjacent Chinese Loess Plateau between 7 and 4 Ma (Passey et al., 2009) which was broadly synchronous with the global increase in the biomass of plants using C_4 photosynthesis between 8 and 6 million year ago (Cerling et al., 1997). Though the triggering mechanism for C_4 expansion is still debatable (Cerling et al., 1997; Pagani et al., 1999), it is agreed that C_4 plants are more favorable at low altitude with warm, water-stressed conditions (Edwards et al., 2010). We take the dominant C_3 plants throughout the Miocene to Quaternary as independent evidence that our study area had been uplifted to high elevations comparable to the present prior to 10 Ma, accompanied by changes in climate not favorable for C_4 plants. In addition, mammal fossil records indicate a change in environment capable of supporting large mammals, like the shovel-tusked elephant *Platybelodon*, primitive horse *Anchitherium*, and endemic bovids prior to 10 Ma to an environment with the dominant presence of dicrocerine deer (Wang et al., 2007). In total, these studies support a transition in ecology and environment corresponding to the uplift and growth in the northern Tibetan Plateau in Middle-Late Miocene.

5.2.3. High elevations in northern Tibetan Plateau by 10.4 Ma

Given previous discussions, we conclude that the major mechanism driving the decrease in δD_m of -50.6‰ during Stage I was due to an altitudinal effect of plateau growth. Theoretically, the isotopic evolution of precipitation during rainout processes is largely controlled by temperature through Rayleigh distillation process (Clark and Fritz, 1997; Dansgaard, 1964; Rowley et al., 2001; Rozanski et al., 1993). As a vapor is lifted orographically, it expands and cools, causing progressive rainout and isotopically depleted precipitation (Clark and Fritz, 1997) – consistent with the coincidence between Middle-Late Miocene active tectonism, the gradual decrease in δD_m , and an inferred regional temperature drop.

The dominant role of altitudinal effects on the isotopic fractionation during precipitations was recorded by studies on modern soils which reveal that sedimentary leaf wax hydrogen isotopes in soils (δD_{n-alk}) track altitudinal variations of hydrogen isotopes in precipitations (δD_m) and show strong dependence of δD_{n-alk} on elevation (Fig. 7a; Bai et al., 2011; Jia et al., 2008; Luo et al., 2011). The most striking is that the gradient of decreasing δD_{n-alk} with increasing elevation is very similar in all transects that span variable environment conditions regardless of moisture sources (Bai et al., 2011; Jia et al., 2008; Luo et al., 2011) and the mean value (-21.6‰/km) is consistent with global meteoric water isotopic lapse rate of $\sim -22.4\text{‰/km}$ (Dansgaard, 1964; Poage

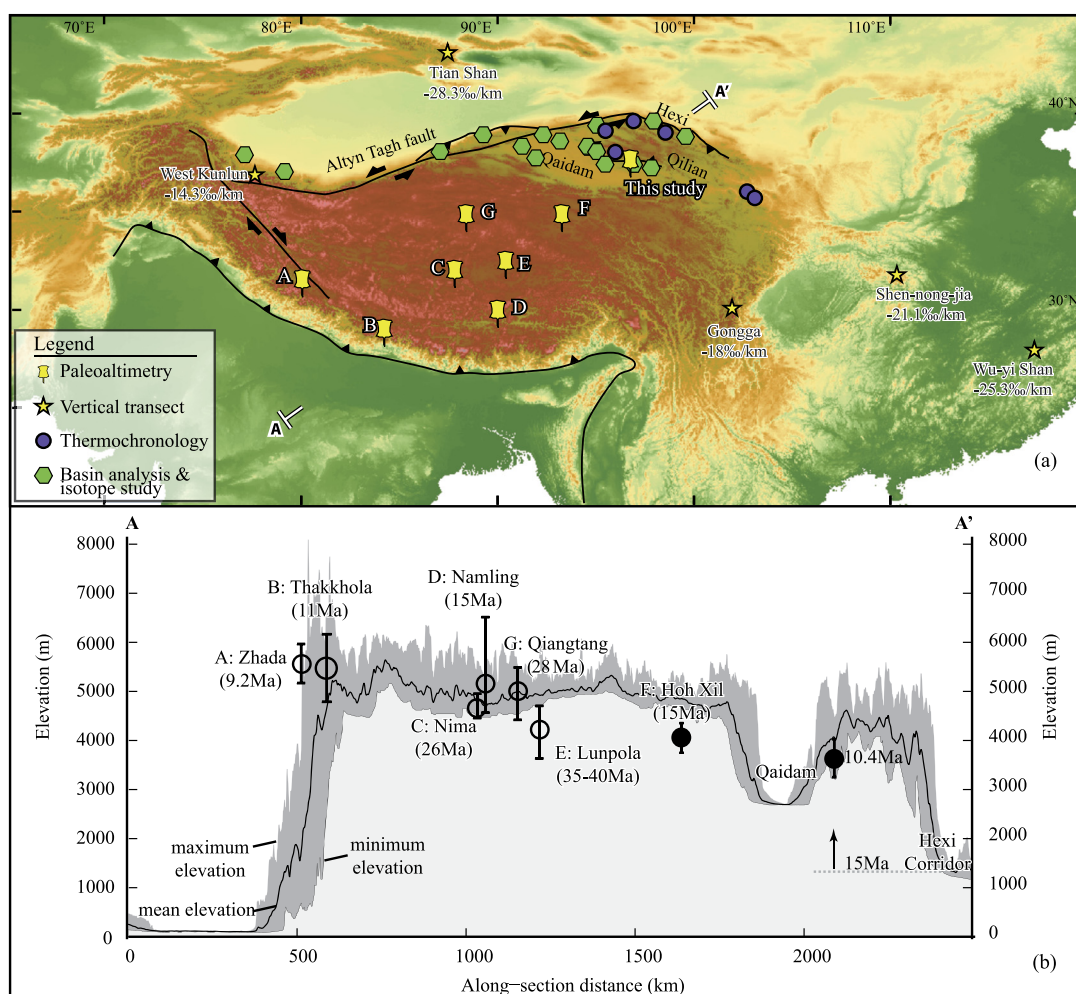


Fig. 8. Paleotopographic development on the Tibetan Plateau. (a) Altitudinal studies on sedimentary leaf wax isotopes (yellow stars) in and around the Tibetan Plateau and geological studies that support Middle-Late Miocene active tectonism. Altitudinal studies are compiled from Bai et al. (2011), Jia et al. (2008), and Luo et al. (2011). Green hexagons indicate basin analysis and isotope studies (Bovet et al., 2009; Kent-Corson et al., 2009; Zhuang et al., 2011a, 2011b). Purple dots are low-temperature thermochronology studies, compiled from George et al. (2001), Johnstone et al. (2009), Lease et al. (2011), and Zheng et al. (2010). The line AA' denotes the location of topographic cross-section shown in (b). (b) Topographic cross-section with projected paleoaltimetry studies, indicating the attainment of high elevations on the plateau prior to 10 Ma. Paleoaltimetry studies in Hoh Xil and Qaidam (black circles) explore the sedimentary leaf wax hydrogen isotope analysis; other paleoaltimetry studies are based on ^{18}O preserved in carbonates. (For interpretation of the references to color in this figure legend, the reader is referred to the web version of this article.)

and Chamberlain, 2001). Luo et al. (2011) reported $-25.3\text{‰}/\text{km}$, $-21.1\text{‰}/\text{km}$, and $-28.6\text{‰}/\text{km}$ with the first two (Wuyi and Shen-nong-jia) from the humid monsoonal area and the third (Tian Shan) from the arid central Asia (Figs. 1 and 7a). Reports from Jia et al. (2008) and Bai et al. (2011) from the Mount Gongga on the southeastern Tibetan Plateau are very consistent with each other with a value of ca. $-18\text{‰}/\text{km}$ (Fig. 7a). Bai et al. (2011) also reported an extreme in the West Kunlun with a smaller gradient (ca. $-14\text{‰}/\text{km}$). We don't have affirmative interpretations on this extreme. However, the above studies demonstrate that sedimentary leaf waxes are ideal archives of precipitations and changes in $\delta D_{n\text{-alk}}$ document elevation variations and hence would be suitable to estimate changes in paleoelevation.

We applied this empirical relationship to evaluate changes in elevations (Fig. 7). The range of $-18\text{‰}/\text{km}$ to $-28.6\text{‰}/\text{km}$, corresponding to the decrease in $\delta D_{n\text{-alk}}$ of -45.5‰ (equal to -50.6‰ in δD_m), would suggest a gain in elevation of 1.6–2.5 km, or 2.1 km for the mean gradient of $-21.6\text{‰}/\text{km}$ (Fig. 7b). The application of a smaller value, for example $-14\text{‰}/\text{km}$ in the extreme case in the West Kunlun, would give a much bigger estimate (>3 km). Interestingly, the inferred change in temperature of 12.3°C provides a similar estimate of 1.9 km in elevation

gain, if a global temperature gradient of $-6.5^\circ\text{C}/\text{km}$ was applied (Barry, 1992). This consistency is not surprising, considering that the isotopic fractionation during rainout processes is largely controlled by temperature (Clark and Fritz, 1997; Dansgaard, 1964; Rowley et al., 2001; Rozanski et al., 1993). The estimate of 2.1 km uplift suffers from potential systematic errors due to the analytical error, moisture source, and apparent fractionation factor. The average analytical error is less than 2.6‰ (1σ). In terms to moisture source, we averaged altitudinal $\delta D_{n\text{-alk}}$ gradients in this region and retained the standard deviation (5.1‰) as a conservative measure of uncertainties associated with moisture sources. Finally, the apparent fractionation between leaf waxes and meteoric waters ($\varepsilon_{n\text{-alk}/m}$) varies among living plants (Magill et al., 2013; Sachse et al., 2012) and could cause a difference of 15–20‰ in δD between different plant communities such as C_3 and C_4 plants (Chikaraishi and Naraoka, 2003; Sachse et al., 2012; Smith and Freeman, 2006). Jia et al. (2012) present isotopic evidence supporting the C_4 to C_3 transition is on the order of 10–20 percent, which contribute no more than 4‰ to the total uncertainty. The combined error would be 7.0‰ , accounting for an uncertainty of ca. 0.3 km in elevation. We suggest the true uncertainty is smaller than this value as we maximize each factor.

Our estimate in surface uplift is equal to the difference in elevation between the present Qaidam and Hexi Corridor (Fig. 8). If we assume that the Qaidam basin started from an elevation similar to the foreland Hexi Corridor, then 2.1-km uplift suggests that Qaidam attained its present high elevation by 10.4 Ma (Fig. 8b). Additional evidence of high elevations in the Qaidam basin comes from the reconstructed δD_m record itself in which no interval following the Stage I shows lower values of reconstructed δD_m (Fig. 6), as if higher elevations were obtained after 10.4 Ma, more negative meteoric water δD values should be observed. A high elevation by 10.4 Ma in the northern Tibetan Plateau is consistent with theoretical predictions which are scaling the attainment of high elevations on the Tibetan plateau with the convergence between Indian and Eurasian plates (Rowley and Currie, 2006) and is synchronous with the marked decline in India–Asia convergence, which was interpreted as a result of attainment of high topography across the plateau (Molnar and Stock, 2009).

5.3. A dynamic climate

Our reconstructed paleometeoric water record also reveals a dynamic climate that shifted between dry and moist conditions, independent of topographic change given that similar high elevations had been obtained prior to 10.4 Ma in this region. Two abrupt increases in δD_m at 10.4 Ma and 4.1 Ma and high δD_m values in Stages II and IV (Fig. 6) reflect the shift in climatic regime from moist to dry conditions. First, the increasing temperature, requested by increases in δD_m , seems to be unlikely considering the persistent global cooling since the Middle Miocene (Flower and Kennett, 1994; Zachos et al., 2001). Second, the rapid decrease in altitude is also an unlikely scenario to interpret abrupt increases in δD_m , as there is no geological evidence for tectonic collapse in the northern Tibetan Plateau since the Middle Miocene. Third, changes in δD_m are not synchronous with and hence have no connection with sedimentary facies changes (Fig. 6). The coincidence in timing, together with isotopic evidence of no significant change in vegetation (Wang and Deng, 2005; Zhang et al., 2012), leads us to conclude that both oxygen and hydrogen isotopic systems record strengthened aridity at ca. 10–8 Ma and since 4 Ma (Dettman et al., 2001; Heermance et al., 2013; Hough et al., 2011; Zhuang et al., 2011a).

We postulate that the 10–8 Ma severe aridity occurred in the context of high elevations on the Tibetan Plateau (Fig. 8) and a weak East Asia Summer Monsoon; shortage of moistures would aggravate with the blockage by high elevations. High δD_m values in dry Stage II have a difference of 25–62‰ in comparison to the most negative value in Stage I (Fig. 6). We apply the δD_m -precipitation relationship ($-0.215\text{‰}/\text{mm}$) and determine a water deficit on the order of 110–290 mm during Stage II. We acknowledge that this is a coarse estimate, but consistent with those calculated from inorganic carbonate records which suggest a water deficit on the order of 200–300 mm (Zhuang et al., 2011a). Similarly, we interpret that high δD_m values in Stage IV (Fig. 6) reflect a drying climate, consistent with oxygen isotopic study on carbonates in the western Qaidam basin (Heermance et al., 2013). δD_m ranges between -31.2‰ and -53.7‰ – slightly higher than modern value of $\sim -55\text{‰}$ (Tian et al., 2001) and suggests Stage IV was drier than today. Further, δD_m values are 28.6–45.1‰ larger than values prior to this stage, suggesting a water deficit on the order of 130–210 mm.

The shifting climatic regime is supported by recent isotopic study on stalagmites and lake sediments which reveals fluctuations in dry and humid conditions in western Qaidam and Tian Shan (Cheng et al., 2012; Wang et al., 2013). The decreasing δD_m around 6.9 Ma and lower δD_m values in Stage III (Fig. 6) reflect a change in climate from dry to humid. A decrease of $\sim -47\text{‰}$

from Stage II to Stage III would be equal to an ~ 220 mm increase in precipitation. The humid Stage III was broadly consistent with the open period in basin hydrography in the Linxia and Xunhua basins on the northeastern corner of Tibetan Plateau, as suggested by low $\delta^{18}\text{O}_{\text{cc}}$ values (Fan et al., 2007; Hough et al., 2011). A wet Stage III is also consistent with stable oxygen isotopic studies on the Chinese Loess Plateau, which support the intensified East Asia Summer Monsoon between 7 Ma and 4 Ma (Passey et al., 2009). This implies that during Stage III the region was under the control of moist monsoon systems associated with isotopically light meteoric waters.

Our interpretation of a dynamic climate is also supported by short-term, high-frequency δD_m variations. For example, during Stage II with a dominant dry climate, high-frequency variations in δD_m could reflect oscillations in climate between very dry (very high δD_m values) and less dry (relatively low δD_m values) conditions – and interpretation broadly consistent with the isotopic study in Linxia Basin that supports oscillations in climate and accompanied changes in lake systems between hydrographically closed and open stages (Fan et al., 2007). Similarly, variations in δD_m during Stage IV could be the result of greater climate variability during the Plio-Pleistocene (Dettman et al., 2003; Fan et al., 2007). Whereas, higher δD_m values at ~ 12.5 Ma and ~ 5.5 Ma (Fig. 6) could reflect transient dry events which were superimposed upon the trend of isotopic depletion related to surface uplift and moist conditions in monsoon-dominant stage, respectively.

6. Concluding remarks

Stable hydrogen isotopic compositions of higher-plant *n*-alkanes were used to reconstruct a 13-million-year-long record of paleometeoric waters on the northern Tibetan Plateau. This time series presents quantitative constraints on topographic development, revealing 2.1 km surface uplift and supporting the attainment of high elevations in Qaidam by 10.4 Ma, posterior to those in the southern and central Tibetan Plateau. Our reconstructed records of meteoric water isotopic compositions indicate that the climate in the northern Tibetan Plateau did not experience permanent drying. On the contrary, our data, together with regional isotopic and pollen studies, reflect a dynamic climate that was characterized by periodic shifts between dry and moist conditions.

Acknowledgements

We would like to thank two anonymous reviewers for their thorough and complete comments and suggestions helped improve the quality of the paper. G. Zhuang thanks the Bateman Postdoctoral Fellowship from Department of Geology and Geophysics of Yale University. We would also like to thank laboratory assistance from Yige Zhang and Peter Douglas. Isotope analysis was conducted at the Earth Systems Center for Stable Isotope Studies (ESCSIS) at Yale University. Glendon Hunsinger is acknowledged for his technical support.

Appendix A. Supplementary material

Supplementary material related to this article can be found online at <http://dx.doi.org/10.1016/j.epsl.2014.01.003>.

References

- Aichner, B., Herzschuh, U., Wilkes, H., Vieth, A., Böhner, J., 2010. δD values of *n*-alkanes in Tibetan lake sediments and aquatic macrophytes – A surface sediment study and application to a 16 ka record from Lake Koucha. *Org. Geochem.* 41, 779–790.

- An, Z., Kutzbach, J.E., Prell, W.L., Porter, S.C., 2001. Evolution of Asian monsoons and phased uplift of the Himalaya–Tibetan plateau since Late Miocene times. *Nature* 411, 62–66.
- Araguás-Araguás, L., Froehlich, K., Rozanski, K., 1998. Stable isotope composition of precipitation over southeast Asia. *J. Geophys. Res.* 103, 28721–28728, 28742.
- Bai, Y., Fang, X., Gleixner, G., Mügler, I., 2011. Effect of precipitation regime on δD values of soil n -alkanes from elevation gradients: Implications for the study of paleo-elevation. *Org. Geochem.* 42, 838–845.
- Bai, Y., Fang, X., Tian, Q., 2012. Spatial patterns of soil n -alkane δD values on the Tibetan Plateau: Implications for monsoon boundaries and paleoelevation reconstructions. *J. Geophys. Res.* 117, D20113.
- Barry, R.G., 1992. *Mountain Weather & Climate*. Psychology Press.
- Bershaw, J., Penny, S.M., Garzione, C.N., 2012. Stable isotopes of modern water across the Himalaya and eastern Tibetan Plateau: Implications for estimates of paleoelevation and paleoclimate. *J. Geophys. Res.* 117, D02110.
- Bi, X., Sheng, G., Liu, X., Li, C., Fu, J., 2005. Molecular and carbon and hydrogen isotopic composition of n -alkanes in plant leaf waxes. *Org. Geochem.* 36, 1405–1417.
- Bovet, P., Ritts, B., Gehrels, G., Abbink, A., Darby, B., Hourigan, J., 2009. Evidence of Miocene crustal shortening in the North Qilian Shan from Cenozoic stratigraphy of the western Hexi Corridor, Gansu Province, China. *Am. J. Sci.* 309, 290–329.
- Bowen, G.J., Revenaugh, J., 2003. Interpolating the isotopic composition of modern meteoric precipitation. *Water Resour. Res.* 39, 1299.
- Cerling, T.E., Harris, J.M., MacFadden, B.J., Leakey, M.G., Quade, J., Eisenmann, V., Ehleringer, J.R., 1997. Global vegetation change through the Miocene/Pliocene boundary. *Nature* 389, 153–158.
- Chang, D., 1981. The vegetation zonation of the Tibetan Plateau. *Mt. Res. Dev.* 29–48.
- Cheng, H., Zhang, P., Spötl, C., Edwards, R., Cai, Y., Zhang, D., Sang, W., Tan, M., An, Z., 2012. The climatic cyclicity in semiarid–arid central Asia over the past 500,000 years. *Geophys. Res. Lett.* 39.
- Chikaraishi, Y., Naraoka, H., 2003. Compound-specific $\delta D \delta^{13}C$ analyses of n -alkanes extracted from terrestrial and aquatic plants. *Phytochemistry* 63, 361–371.
- Chikaraishi, Y., Naraoka, H., Poulson, S.R., 2004. Hydrogen and carbon isotopic fractionations of lipid biosynthesis among terrestrial (C3, C4 and CAM) and aquatic plants. *Phytochemistry* 65, 1369–1381.
- Clark, I.D., Fritz, P., 1997. *Environmental Isotopes in Hydrogeology*. CRC Press.
- Clark, M.K., Farley, K.A., Zheng, D., Wang, Z., Duvall, A.R., 2010. Early Cenozoic faulting of the northern Tibetan Plateau margin from apatite (U–Th)/He ages. *Earth Planet. Sci. Lett.* 296, 78–88.
- Cooper, J., Bray, E., 1963. A postulated role of fatty acids in petroleum formation. *Geochim. Cosmochim. Acta* 27, 1113–1127.
- Currie, B., Rowley, D., Tabor, N., 2005. Middle Miocene paleoaltimetry of southern Tibet: Implications for the role of mantle thickening and delamination in the Himalayan orogen. *Geology* 33, 181.
- Dansgaard, W., 1964. Stable isotopes in precipitation. *Tellus* 16, 436–468.
- DeCelles, P., Robinson, D., Zandt, G., 2002. Implications of shortening in the Himalayan fold-thrust belt for uplift of the Tibetan Plateau. *Tectonics* 21, 1062.
- DeCelles, P., Quade, J., Kapp, P., Fan, M., Dettman, D., Ding, L., 2007. High and dry in central Tibet during the Late Oligocene. *Earth Planet. Sci. Lett.* 253, 389–401.
- Dettman, D.L., Kohn, M.J., Quade, J., Ryerson, F., Ojha, T.P., Hamidullah, S., 2001. Seasonal stable isotope evidence for a strong Asian monsoon throughout the past 10.7 my. *Geology* 29, 31–34.
- Dettman, D., Fang, X., Garzione, C., Li, J., 2003. Uplift-driven climate change at 12 Ma: a long $\delta^{18}O$ record from the NE margin of the Tibetan plateau. *Earth Planet. Sci. Lett.* 214, 267–277.
- Douglas, P., Pagani, M., Brenner, M., Hodell, D., Curtis, J., 2012. Aridity and vegetation composition are important determinants of leaf-wax δD values in southeastern Mexico and Central America. *Geochim. Cosmochim. Acta*.
- Edwards, E.J., Osborne, C.P., Strömberg, C.A., Smith, S.A., 2010. The origins of C4 grasslands: integrating evolutionary and ecosystem science. *Science* 328, 587–591.
- Eglinton, G., Hamilton, R.J., 1967. Leaf epicuticular waxes. *Science* 156, 1322.
- Fan, M., Dettman, D.L., Song, C., Fang, X., Garzione, C.N., 2007. Climatic variation in the Linxia basin, NE Tibetan Plateau, from 13.1 to 4.3 Ma: The stable isotope record. *Palaeogeogr. Palaeoclimatol. Palaeoecol.* 247, 313–328.
- Fang, X., Zhang, W., Meng, Q., Gao, J., Wang, X., King, J., Song, C., Dai, S., Miao, Y., 2007. High-resolution magnetostratigraphy of the Neogene Huaitoutala section in the eastern Qaidam Basin on the NE Tibetan Plateau, Qinghai Province, China and its implication on tectonic uplift of the NE Tibetan Plateau. *Earth Planet. Sci. Lett.* 258, 293–306.
- Flower, B.P., Kennett, J.P., 1994. The middle Miocene climatic transition: East Antarctic ice sheet development, deep ocean circulation and global carbon cycling. *Palaeogeogr. Palaeoclimatol. Palaeoecol.* 108, 537–555.
- Garzione, C.N., Dettman, D.L., Quade, J., DeCelles, P.G., Butler, R.F., 2000a. High times on the Tibetan Plateau: Paleoelevation of the Thakkhola graben, Nepal. *Geology* 28, 339–342.
- Garzione, C.N., Quade, J., DeCelles, P.G., English, N.B., 2000b. Predicting paleoelevation of Tibet and the Himalaya from $\delta^{18}O$ vs. altitude gradients in meteoric water across the Nepal Himalaya. *Earth Planet. Sci. Lett.* 183, 215–229.
- George, A., Marshall, S., Wyrwoll, K., Jie, C., Yanchou, L., 2001. Miocene cooling in the northern Qilian Shan, northeastern margin of the Tibetan Plateau, revealed by apatite fission-track and vitrinite-reflectance analysis. *Geology* 29, 939.
- Gonfiantini, R., Roche, M.A., Olivry, J.C., Fontes, J.C., Zuppi, G.M., 2001. The altitude effect on the isotopic composition of tropical rains. *Chem. Geol.* 181, 147–167.
- Graham, S., Chamberlain, C., Yue, Y., Ritts, B., Hanson, A., Horton, T., Waldbauer, J., Poage, M., Feng, X., 2005. Stable isotope records of Cenozoic climate and topography, Tibetan plateau and Tarim basin. *Am. J. Sci.* 305, 101–118.
- Heermance, R.V., Pullen, A., Kapp, P., Garzione, C.N., Bogue, S., Ding, L., Song, P., 2013. Climatic and tectonic controls on sedimentation and erosion during the Pliocene–Quaternary in the Qaidam Basin (China). *Geol. Soc. Am. Bull.* 125, 833–856.
- Hou, J., D’Andrea, W.J., Huang, Y., 2008. Can sedimentary leaf waxes record DH ratios of continental precipitation? Field, model, and experimental assessments. *Geochim. Cosmochim. Acta* 72, 3503–3517.
- Hough, B.G., Garzione, C.N., Wang, Z., Lease, R.O., Burbank, D.W., Yuan, D., 2011. Stable isotope evidence for topographic growth and basin segmentation: Implications for the evolution of the NE Tibetan Plateau. *Bull. Geol. Soc. Am.* 123, 168.
- Hren, M.T., Bookhagen, B., Blisniuk, P.M., Booth, A.L., Chamberlain, C.P., 2009. $\delta^{18}O$ and δD of streamwaters across the Himalaya and Tibetan Plateau: Implications for moisture sources and paleoelevation reconstructions. *Earth Planet. Sci. Lett.* 288, 20–32.
- Hren, M.T., Pagani, M., Erwin, D.M., Brandon, M., 2010. Biomarker reconstruction of the early Eocene paleotopography and paleoclimate of the northern Sierra Nevada. *Geology* 38, 7–10.
- IAEA/WMO, 2006. *Global network of isotopes in precipitation: The GNIP database*. <http://isohis.iaea.org>.
- Jia, G., Wei, K., Chen, F., Peng, P., 2008. Soil n -alkane δD vs. altitude gradients along Mount Gongga, China. *Geochim. Cosmochim. Acta* 72, 5165–5174.
- Jia, G., Li, Z., Peng, P., Zhou, L., 2012. Aeolian n -alkane isotopic evidence from North Pacific for a Late Miocene decline of C4 plant in the arid Asian interior. *Earth Planet. Sci. Lett.* 321, 32–40.
- Johnstone, S., Hourigan, J., Zhuang, G., Ritts, B., Darby, B., 2009. Miocene exhumation of the Northern and Southern Qilian Shan, N. China: results from apatite U–Th/He thermochronology. In: *AGU Fall Meeting Abstracts* 1, p. 2066.
- Jolivet, M., Brunel, M., Seward, D., Xu, Z., Yang, J., Roger, F., Tapponnier, P., Malavieille, J., Arnaud, N., Wu, C., 2001. Mesozoic and Cenozoic tectonics of the northern edge of the Tibetan plateau: fission-track constraints. *Tectonophysics* 343, 111–134.
- Kent-Corson, M., Ritts, B., Zhuang, G., Bovet, P., Graham, S., Page Chamberlain, C., 2009. Stable isotopic constraints on the tectonic, topographic, and climatic evolution of the northern margin of the Tibetan Plateau. *Earth Planet. Sci. Lett.* 282, 158–166.
- Kutzbach, J.E., Guetter, P.J., Ruddiman, W.F., Prell, W.L., 1989. Sensitivity of climate to late Cenozoic uplift in Southern Asia and the American West: Numerical experiments. *J. Geophys. Res.* 94, 18393–18407.
- Kutzbach, J.E., Prell, W.L., Ruddiman, W.F., 1993. Sensitivity of Eurasian climate to surface uplift of the Tibetan Plateau. *J. Geol.* 101, 177–190.
- Lease, R.O., Burbank, D.W., Gehrels, G.E., Wang, Z., Yuan, D., 2007. Signatures of mountain building: Detrital zircon U/Pb ages from northeastern Tibet. *Geology* 35, 239–242.
- Lease, R.O., Burbank, D.W., Clark, M.K., Farley, K.A., Zheng, D., Zhang, H., 2011. Middle Miocene reorganization of deformation along the northeastern Tibetan Plateau. *Geology* 39, 359.
- Liu, W., Yang, H., 2008. Multiple controls for the variability of hydrogen isotopic compositions in higher plant n -alkanes from modern ecosystems. *Glob. Change Biol.* 14, 2166–2177.
- Loader, C., 1999. *Local Regression and Likelihood*. Springer-Verlag.
- Luo, P., Peng, P., Gleixner, G., Zheng, Z., Pang, Z., Ding, Z., 2011. Empirical relationship between leaf wax n -alkane δD and altitude in the Wuyi, Shennongjia and Tianshan Mountains, China: Implications for paleoaltimetry. *Earth Planet. Sci. Lett.* 301, 285–296.
- Magill, C.R., Ashley, G.M., Freeman, K.H., 2013. Water, plants, and early human habitats in eastern Africa. *Proc. Natl. Acad. Sci. USA* 110, 1175–1180.
- Marzi, R., Torkelson, B., Olson, R., 1993. A revised carbon preference index. *Org. Geochem.* 20, 1303–1306.
- McInerney, F.A., Helliker, B.R., Freeman, K.H., 2011. Hydrogen isotope ratios of leaf wax n -alkanes in grasses are insensitive to transpiration. *Geochim. Cosmochim. Acta* 75, 541–554.
- Miao, Y., Fang, X., Herrmann, M., Wu, F., Zhang, Y., Liu, D., 2010. Miocene pollen record of KC-1 core in the Qaidam Basin, NE Tibetan Plateau and implications for evolution of the East Asian monsoon. *Palaeogeogr. Palaeoclimatol. Palaeoecol.*
- Molnar, P., England, P., 1990. Late Cenozoic uplift of mountain ranges and global climate change: chicken or egg? *Nature* 346, 29–34.
- Molnar, P., Stock, J., 2009. Slowing of India’s convergence with Eurasia since 20 Ma and its implications for Tibetan mantle dynamics. *Tectonics* 28.
- Molnar, P., England, P., Martinod, J., 1993. Mantle dynamics, uplift of the Tibetan Plateau, and the Indian monsoon. *Rev. Geophys.* 31, 357–396.

- Mosbrugger, V., Utescher, T., Dilcher, D.L., 2005. Cenozoic continental climatic evolution of Central Europe. *Proc. Natl. Acad. Sci. USA* 102, 14964–14969.
- Murphy, M., Yin, A., Harrison, T., Dürr, S., Chen, Z., Ryerson, F., Kidd, W., Wang, X., Zhou, X., 1997. Did the Indo-Asian collision alone create the Tibetan plateau? *Geology* 25, 719–722.
- Pagani, M., Freeman, K.H., Arthur, M.A., 1999. Late Miocene atmospheric CO₂ concentrations and the expansion of C₄ grasses. *Science* 285, 876–879.
- Pagani, M., Freeman, K.H., Arthur, M.A., 2000. Isotope analyses of molecular and total organic carbon from Miocene sediments. *Geochim. Cosmochim. Acta* 64, 37–49.
- Passey, B.H., Ayliffe, L.K., Kaakinen, A., Zhang, Z., Eronen, J.T., Zhu, Y., Zhou, L., Cerling, T.E., Fortelius, M., 2009. Strengthened East Asian summer monsoons during a period of high-latitude warmth? Isotopic evidence from Mio-Pliocene fossil mammals and soil carbonates from northern China. *Earth Planet. Sci. Lett.* 277, 443–452.
- Poage, M.A., Chamberlain, C.P., 2001. Empirical relationships between elevation and the stable isotope composition of precipitation and surface waters: considerations for studies of paleoelevation change. *Am. J. Sci.* 301, 1–15.
- Polissar, P.J., Freeman, K.H., 2010. Effects of aridity and vegetation on plant-wax δD in modern lake sediments. *Geochim. Cosmochim. Acta* 74, 5785–5797.
- Polissar, P.J., Freeman, K.H., Rowley, D.B., McInerney, F.A., Currie, B.S., 2009. Paleoaltimetry of the Tibetan Plateau from D/H ratios of lipid biomarkers. *Earth Planet. Sci. Lett.* 287, 64–76.
- Quade, J., Garzione, C., Eiler, J., 2007. Paleoelevation reconstruction using pedogenic carbonates. *Rev. Mineral. Geochem.* 66, 53.
- Quade, J., Breecker, D.O., Daëron, M., Eiler, J., 2011. The paleoaltimetry of Tibet: An isotopic perspective. *Am. J. Sci.* 311, 77–115.
- Raymo, M.E., Ruddiman, W.F., 1992. Tectonic forcing of late Cenozoic climate. *Nature* 359, 117–122.
- Reiners, P., Brandon, M., 2006. Using thermochronology to understand orogenic erosion. *Annu. Rev. Earth Planet. Sci.* 34, 419.
- Rowley, D.B., Currie, B.S., 2006. Palaeo-altimetry of the late Eocene to Miocene Lunpola basin, central Tibet. *Nature* 439, 677–681.
- Rowley, D.B., Pierrehumbert, R.T., Currie, B.S., 2001. A new approach to stable isotope-based paleoaltimetry: implications for paleoaltimetry and paleohypsometry of the High Himalaya since the Late Miocene. *Earth Planet. Sci. Lett.* 188, 253–268.
- Rowley, D.B., Currie, B.S., Pierrehumbert, R.T., 2003. Reply to “Modern precipitation stable isotope vs. elevation gradients in the High Himalaya” by Hou Shugui et al. *Earth Planet. Sci. Lett.* 209, 401–403.
- Royden, L.H., Burchfiel, B.C., van der Hilst, R.D., 2008. The Geological Evolution of the Tibetan Plateau. *Science* 321, 1054–1058.
- Rozanski, K., Araguas-Araguas, L., Gonfiantini, R., 1993. Isotopic patterns in modern global precipitation. In: *Climate Change in Continental Isotope Records*, vol. 78, pp. 1–36.
- Ruddiman, W., Kutzbach, J., 1989. Forcing of late Cenozoic Northern Hemisphere climate by plateau uplift in southern Asia and the American west. *J. Geophys. Res.* 94, 18409–18427.
- Sachse, D., Radke, J., Gleixner, G., 2004. Hydrogen isotope ratios of recent lacustrine sedimentary *n*-alkanes record modern climate variability. *Geochim. Cosmochim. Acta* 68, 4877–4889.
- Sachse, D., Billault, I., Bowen, G.J., Chikaraishi, Y., Dawson, T.E., Feakins, S.J., Freeman, K.H., Magill, C.R., McInerney, F.A., Van der Meer, M.T., 2012. Molecular paleohydrology: interpreting the hydrogen-isotopic composition of lipid biomarkers from photosynthesizing organisms. *Annu. Rev. Earth Planet. Sci.* 40, 221–249.
- Sauer, P.E., Eglinton, T.L., Hayes, J.M., Schimmelmann, A., Sessions, A.L., 2001. Compound-specific D/H ratios of lipid biomarkers from sediments as a proxy for environmental and climatic conditions. *Geochim. Cosmochim. Acta* 65, 213–222.
- Saylor, J., Quade, J., Dettman, D., DeCelles, P., Kapp, P., Ding, L., 2009. The late Miocene through present paleoelevation history of southwestern Tibet. *Am. J. Sci.* 309, 1.
- Schimmelmann, A., Sessions, A.L., Mastalerz, M., 2006. Hydrogen isotopic (D/H) composition of organic matter during diagenesis and thermal maturation. *Annu. Rev. Earth Planet. Sci.* 34, 501–533.
- Sessions, A.L., Burgoyne, T.W., Hayes, J.M., 2001. Correction of H₂⁺ contributions in hydrogen isotope ratio monitoring mass spectrometry. *Anal. Chem.* 73, 192–199.
- Smith, F.A., Freeman, K.H., 2006. Influence of physiology and climate on δD of leaf wax *n*-alkanes from C₃ and C₄ grasses. *Geochim. Cosmochim. Acta* 70, 1172–1187.
- Sun, J., Zhu, R., An, Z., 2005. Tectonic uplift in the northern Tibetan Plateau since 13.7 Ma ago inferred from molasse deposits along the Altyn Tagh Fault. *Earth Planet. Sci. Lett.* 235, 641–653.
- Tapponnier, P., Zhiqin, X., Roger, F., Meyer, B., Arnaud, N., Wittlinger, G., Jingsui, Y., 2001. Oblique stepwise rise and growth of the Tibet Plateau. *Science* 294, 1671–1677.
- Tian, L., Masson-Delmotte, V., Stievenard, M., Yao, T., Jouzel, J., 2001. Tibetan Plateau summer monsoon northward extent revealed by measurements of water stable isotopes. *J. Geophys. Res., Atmos.* 106, 28.
- Tian, L., Yao, T., Schuster, P., White, J., Ichiyanagi, K., Pendall, E., Pu, J., Yu, W., 2003. Oxygen-18 concentrations in recent precipitation and ice cores on the Tibetan Plateau. *J. Geophys. Res.* 108, 4293–4302.
- Tipple, B.J., Pagani, M., 2007. The early origins of terrestrial C₄ photosynthesis. *Annu. Rev. Earth Planet. Sci.* 35, 435–461.
- Tissot, B.P., Welte, D.H., 1978. *Petroleum Formation and Occurrence: A New Approach to Oil and Gas Exploration*.
- Wang, Y., Deng, T., 2005. A 25 my isotopic record of paleodiet and environmental change from fossil mammals and paleosols from the NE margin of the Tibetan Plateau. *Earth Planet. Sci. Lett.* 236, 322–338.
- Wang, X., Qiu, Z., Li, Q., Wang, B., Downs, W.R., Xie, G., Xie, J., Deng, T., Takeuchi, G.T., 2007. Vertebrate paleontology, biostratigraphy, geochronology, and paleoenvironment of Qaidam Basin in northern Tibetan Plateau. *Palaeogeogr. Palaeoclimatol. Palaeoecol.* 254, 363–385.
- Wang, Z., Liu, W., Liu, Z., Wang, H., He, Y., Zhang, F., 2013. A 1700-year *n*-alkanes hydrogen isotope record of moisture changes in sediments from Lake Sugan in the Qaidam Basin, northeastern Tibetan Plateau. *Holocene*.
- Xu, Q., Ding, L., Zhang, L., Cai, F., Lai, Q., Yang, D., Liu-Zeng, J., 2013. Paleogene high elevations in the Qiangtang Terrane, central Tibetan Plateau. *Earth Planet. Sci. Lett.* 362, 31–42.
- Yin, A., Rumelhart, P., Butler, R., Cowgill, E., Harrison, T., Foster, D., Ingersoll, R., Qing, Z., Xian-Qiang, Z., Xiao-Feng, W., 2002. Tectonic history of the Altyn Tagh fault system in northern Tibet inferred from Cenozoic sedimentation. *Geol. Soc. Am. Bull.* 114, 1257–1295.
- Yue, Y., Ritts, B., Graham, S., Wooden, J., Gehrels, G., Zhang, Z., 2003. Slowing extrusion tectonics: lowered estimate of post-Early Miocene slip rate for the Altyn Tagh fault. *Earth Planet. Sci. Lett.* 217, 111–122.
- Yue, Y., Ritts, B., Hanson, A., Graham, S., 2004. Sedimentary evidence against large strike-slip translation on the Northern Altyn Tagh fault, NW China. *Earth Planet. Sci. Lett.* 228, 311–323.
- Zachos, J., Pagani, M., Sloan, L., Thomas, E., Billups, K., 2001. Trends, rhythms, and aberrations in global climate 65 Ma to present. *Science* 292, 686–693.
- Zhang, C., Wang, Y., Li, Q., Wang, X., Deng, T., Tseng, Z.J., Takeuchi, G.T., Xie, G., Xu, Y., 2012. Diets and environments of late Cenozoic mammals in the Qaidam Basin, Tibetan Plateau: Evidence from stable isotopes. *Earth Planet. Sci. Lett.* 333, 70–82.
- Zheng, D., Clark, M., Zhang, P., Zheng, W., Farley, K., 2010. Erosion, fault initiation and topographic growth of the North Qilian Shan (northern Tibetan Plateau). *Geosphere*.
- Zhou, J., Xu, F., Wang, T., Cao, A., Yin, C., 2006. Cenozoic deformation history of the Qaidam Basin, NW China: Results from cross-section restoration and implications for Qinghai–Tibet Plateau tectonics. *Earth Planet. Sci. Lett.* 243, 195–210.
- Zhuang, G., Hourigan, J., Ritts, B., Johnstone, S., 2009. Mesozoic to Cenozoic Tectonics of Northern Qaidam Basin, Northern Tibetan Plateau, constrained by apatite (U–Th)/He thermochronology and Basin Analysis. In: *AGU Fall Meeting Abstracts* 1, p. 2105.
- Zhuang, G., Hourigan, J.K., Koch, P.L., Ritts, B.D., Kent-Corson, M.L., 2011a. Isotopic constraints on intensified aridity in Central Asia around 12 Ma. *Earth Planet. Sci. Lett.* 312, 152–163.
- Zhuang, G., Hourigan, J.K., Ritts, B.D., Kent-Corson, M.L., 2011b. Cenozoic multiple-phase tectonic evolution of the northern Tibetan Plateau: Constraints from sedimentary records from Qaidam basin, Hexi Corridor, and Subei basin, northwest China. *Am. J. Sci.* 311, 116–152.